J. Phys.: Condens. Matter **21** (2009) 216001 (10pp) doi:10.1088/0953-8984/21/21/216001

Spin rotation technique for non-collinear magnetic systems: application to the generalized Villain model

J T Haraldsen and R S Fishman

Materials Science and Technology Division, Oak Ridge National Laboratory, Oak Ridge, TN 37831, USA

Received 12 December 2008, in final form 11 March 2009
Published 24 April 2009
Online at stacks.iop.org/JPhysCM/21/216001

Abstract

This work develops a generalized technique for determining the static and dynamic properties of any non-collinear magnetic system. By rotating the spin operators into the local spin reference frame, we evaluate the zeroth, first, and second order terms in a Holstein–Primakoff expansion, and through a Green's functions approach, we determine the structure factor intensities for the spin-wave frequencies. To demonstrate this technique, we examine the spin-wave dynamics of the generalized Villain model with a varying interchain interaction. The new interchain coupling expands the overall phase diagram with the realization of two non-equivalent canted spin configurations. The rotational Holstein–Primakoff expansion provides both analytical and numerical results for the spin dynamics and intensities of these phases.

(Some figures in this article are in colour only in the electronic version)

1. Introduction

Disordered and frustrated magnetic systems have provided condensed-matter physics with a range of complicated problems [1]. Magnetic frustration is typically induced by competing nearest-neighbor and next-nearest-neighbor antiferromagnetic (AF) interactions [1, 2]. To minimize the energy, the local moments frequently rotate into a non-collinear ground-state configuration [2, 3]. Theoretical and experimental efforts have worked to identify and characterize non-collinear magnetic systems. Quantum Monte Carlo and Hartree–Fock calculations have been used to describe canted antiferromagnetic (CAF) phases in double quantum dots and bi-layer quantum Hall systems [4, 5], while *ab initio* methods have been used to examine non-collinearity in magnetic atomic chains [6]. Through neutron-diffraction studies, layered borocarbide systems RB_2C (R = Dy, Ho, and Er) have demonstrated conventional and unconventional magnetic correlations [7]. Other systems such as the cuprate, ruthenate, and manganite systems (where the competition between AF and ferromagnetic (FM) order have been examined in great depth [13–15]) also display non-collinear characteristics [8–15]. To help understand collinear and non-collinear magnetic systems, we present a general rotational technique for modeling the static and dynamic properties of canted local moments in any periodic system.

This technique employs a rotation of the spin operators in the local reference frame using two angle rotations (θ and ψ) at each site. After this rotation, we use a Holstein–Primakoff (HP) expansion to determine the classical spin energy and the spin-wave (SW) frequencies. By solving the equations-of-motion for coupled Green's functions, we determine the structure factor (SF) intensities for any eigenfrequency of the system. This type of rotational technique has been employed before in many systems ranging from finite cluster models [16] to the SW modes of spin glasses and other non-collinear magnetic systems [17–22]. Walker and Walstedt investigated the dynamics of multiple spin glass ground states by numerical analysis and simulation [20, 21]. The SWs for non-collinear helical phases were examined by Rastelli *et al* incorporating one canting angle and applying it to multiple lattices [22]. While these techniques are similar, we introduce a fully generalized model designed to easily describe the SW and SF intensities in any magnetic system regardless of rotation, arbitrary exchange coupling, and single-ion anisotropy. Here, the inputs into this method are simply the interaction parameters and moment angles; the outputs are the SW frequencies and intensities.

To demonstrate this general technique, we investigate the generalized Villain model with an added interchain coupling. In recent years, the generalized Villain model

 © 2009 IOP Publishing Ltd Printed in the UK

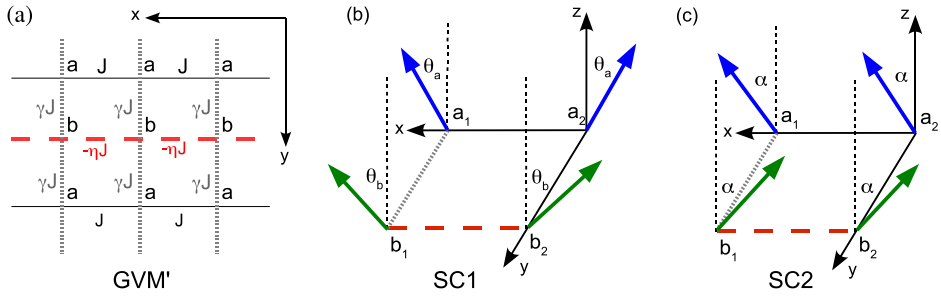

Figure 1. (a) The generalized Villain model (GVM′) with Heisenberg interactions J, γJ, and $-\eta J$. (b) The GVM′ with anti-parallel spin configuration (SC1), where the local moments of sites a and b reside in the xz-plane and are described by the angles (θ_a, θ_b). (c) The GVM′ with parallel spin configuration (SC2), where the local moments of sites a and b reside in the xz-plane and are canted by the angle α. Note that SC2 with $\alpha = \pi/2$ is rotationally equivalent to SC1 with $(0, \pi)$.

(GVM) has been frequently used to test approaches to study magnetically frustrated systems and to help understand more complicated magnetic systems similar to those mentioned above [18, 23–25]. In the GVM, chains of FM interactions J and AF interactions $-\eta J$ along the x-axis are coupled together in the y direction by J [18, 23–25], as illustrated in figure 1(a). The original Villain model assumed that $\eta = 1$, which denotes full frustration [2]. This model was generalized to $\eta \neq 1$ by Berge *et al* [3], accounting for coupling of different magnitudes within the FM and AF chains. Within the GVM, a CAF phase is stabilized for $\eta > \eta_c$. The critical value increases with applied magnetic field from a value of $\eta_c = 1/3$ in zero field. In 1992, Saslow and Erwin [18] employed a HP expansion to numerically examine the SW and SF intensities for this generalized model.

In this paper, the GVM is extended further by introducing a variable y-axis coupling γJ, as shown in figure 1(a). We call this model the GVM′. Therefore, the GVM′ with $\gamma = 1$ reduces to the GVM discussed previously [18, 23–25]. As in the GVM, all interactions are confined to the xy plane but the magnetic is applied along the z-axis. Through an examination of the classical energies, we demonstrate that there exists two separate canted spin configurations throughout $\{\eta, \gamma\}$ phase space. Figures 1(b) and (c) show the possible canted spin configurations within the GVM′. In figure 1(b), the local moments are canted in the xz-plane by angles θ_a and θ_b. In this configuration, the spins projected onto the xy plane are anti-parallel on sites a_1 and a_2 as well as on sites b_1 and b_2 [18, 23–25]. This canted spin configuration occurs in the GVM with $\gamma = 1$. With the introduction of the variable γ, a new spin configuration arises: the corresponding projected moments are parallel with moment angles (α), as shown in figure 1(c). For notational convenience, we call these SC1 (spin configuration 1) for the anti-parallel case (figure 1(b)) and SC2 (spin configuration 2) for the parallel case (figure 1(c)).

Through an examination of the classical limit, we determine the phase diagram within the parameter space $\{\eta, \gamma\}$. The GVM′ is found to support three phases (FM, SC1, and SC2). Using the rotational Holstein–Primakoff expansion, the SW frequencies are determined analytically for all phases. The SF intensities for the FM and zero-field SC2 phases are determined exactly; the rest are solved numerically.

2. The general rotation model

As described in [24], the Hamiltonian for canted magnetic systems can be simplified by rotating into the reference frame for each moment: $\bar{\mathbf{S}}_i = \underline{U}_i \mathbf{S}_i$, where $\underline{U}_i$ is the unitary rotation matrix for site i (discussed in appendix A). In the classical limit, $\bar{\mathbf{S}}_i$ points along its local z-axis. The general Hamiltonian is given by

$$\begin{aligned} H &= -\tfrac{1}{2}\sum_{i\neq j} J_{ij}\mathbf{S}_i \cdot \mathbf{S}_j - \sum_i D_i \mathbf{S}_{iz}^2 - B\sum_i \mathbf{S}_{iz} \\ &= -\tfrac{1}{2}\sum_{i\neq j} J_{ij}\bar{\mathbf{S}}_i \cdot \underline{U}_i\underline{U}_j^{-1}\bar{\mathbf{S}}_j - \sum_i D_i(\underline{U}_i^{-1}\bar{\mathbf{S}}_i)_z^2 \\ &\quad - B\sum_i (\underline{U}_i^{-1}\bar{\mathbf{S}}_i)_z, \end{aligned} \tag{1}$$

where $\mathbf{S}_i$ are the local moments for site i, J_{ij} is the interaction between sites i and j, D_i is the single-ion anisotropy, and B is the applied magnetic field. It should be noted that $\underline{U}_i$ only depends on the moment angles of the spins at site i. The canting of a local moment can be described as a rotation by θ in the xz-plane, with another rotation by ψ in the xy-plane. Therefore, each local moment can be described by the Euler angles θ and ψ [26]. The Hamiltonian is expanded in powers of $1/\sqrt{S}$ about the classical or high-spin limit: $H = E_0 + H_1 + H_2 + \cdots$. Within the HP formalism, the spin operators in the local reference frames become: $\bar{S}_{iz} = S - a_i^\dagger a_i$, $\bar{S}_{i+} = \sqrt{2S}a_i$ and $\bar{S}_{i-} = \sqrt{2S}a_i^\dagger$ [1]. The zeroth order E_0 term corresponds to the classical energy and the second order term H_2 describes the dynamics of non-interacting SWs. The first order term H_1 vanishes when the local moments minimize the classical energy E_0 for a specific interaction pair η and γ. Each term, up to second order, is discussed further below. Higher order terms correspond to SW interactions that are unimportant at low temperatures and for small $1/S$.

2.1. Zeroth order: classical energy

From the above Hamiltonian, the zeroth order terms describe the classical energy and can be written as

$$\begin{aligned} E_0 &= -\tfrac{1}{2}\sum_{i,j} J_{ij}S_iS_jF_{zz}^{ij} - \sum_i D_iS_i^2\cos(\theta_i)^2 \\ &\quad - B'\sum_i S_i^2\cos(\theta_i), \end{aligned} \tag{2}$$

where S_i is the moment magnitude for site i, $B' \equiv B/JS$, and F_{zz}^{ij} is a rotation coefficient given by the angle rotation matrix in appendix A. It only depends on the angles of the spins on sites i and j. From an examination of the global minima, the appropriate spin configuration can be determined by minimizing this classical energy.

2.2. First order: linear terms

The HP expansion produces terms that are linear with respect to the creation and annihilation operators. Therefore, the first order Hamiltonian is given by

$$H_1 = -\sum_{i,j}\frac{S_iS_j}{\sqrt{2}}J_{ij} \times\left(\frac{1}{\sqrt{S_i}}(F_1^{ij}a_i^\dagger + F_1^{ij*}a_i) + \frac{1}{\sqrt{S_j}}(F_2^{ij}a_j^\dagger + F_2^{ij*}a_j)\right) + \sum_i\sqrt{\frac{S_i^3}{2}}\left(B + D_i\sin(2\theta_i)\right)(a_i^\dagger + a_i), \quad (3)$$

where $F_1^{ij} = F_{xz}^{ij} + \mathrm{i}F_{yz}^{ij}$ and $F_2^{ij} = F_{zx}^{ij} + \mathrm{i}F_{zy}^{ij}$. Here, F_{xz}^{ij}, F_{zx}^{ij}, F_{yz}^{ij}, and F_{zy}^{ij} are rotation coefficients that depend only on the moment angles for the interacting spins on sites i and j (described in appendix A). The linear terms correspond to the creation and annihilation of SW's from the vacuum. Assuming the system is in a proper ground state with the angles that minimize the energy, the nonphysical first order coefficients of a_i and $a_i^\dagger$ must vanish for each spin site.

2.3. Second order: spin dynamics and structure factor intensities

The second order terms in the HP expansion describe the spin dynamics. We Fourier transform the spin operators by: $a_{\mathbf{k}}^{(r)} = 1/N\sum_i^{(r)}\mathrm{e}^{-\mathrm{i}\mathbf{k}\cdot\mathbf{R}_i}a_i$ and $a_{\mathbf{k}}^{(r)\dagger} = 1/N\sum_i^{(r)}\mathrm{e}^{\mathrm{i}\mathbf{k}\cdot\mathbf{R}_i}a_i^\dagger$, where the sums are restricted to sub-lattice (SL) r. For each SL of the system, the moment angles are the same. The second order terms of the generalized Hamiltonian can then be written as

$$H_2 = \sum_{r,s}\sum_{u,\mathbf{k}} z_{rs}^{(u)}J_{rs}^{(u)}\sqrt{S_rS_s} \times\left\{\Gamma_{\mathbf{k}}^{rs(u)}\left(G_1^{rs}a_{\mathbf{k}}^{(r)\dagger}a_{\mathbf{k}}^{(s)} + G_2^{rs}a_{\mathbf{k}}^{(r)}a_{-\mathbf{k}}^{(s)}\right) + \Gamma_{\mathbf{k}}^{rs(u)*}\left(G_1^{rs*}a_{\mathbf{k}}^{(r)}a_{\mathbf{k}}^{(s)\dagger} + G_2^{rs*}a_{\mathbf{k}}^{(r)\dagger}a_{-\mathbf{k}}^{(s)\dagger}\right) + F_{zz}^{rs}\left(a_{\mathbf{k}}^{(r)\dagger}a_{\mathbf{k}}^{(r)} + a_{\mathbf{k}}^{(s)\dagger}a_{\mathbf{k}}^{(s)}\right)\right\} - \tfrac{1}{2}\sum_{r,\mathbf{k}}D_rS_r\left\{\sin(\theta_r)^2 \times\left(a_{\mathbf{k}}^{(r)\dagger}a_{-\mathbf{k}}^{(r)\dagger} + a_{\mathbf{k}}^{(r)}a_{-\mathbf{k}}^{(r)} + a_{\mathbf{k}}^{(r)}a_{\mathbf{k}}^{(r)\dagger} + a_{\mathbf{k}}^{(r)\dagger}a_{\mathbf{k}}^{(r)}\right) - 4\cos(\theta_r)^2a_{\mathbf{k}}^{(r)\dagger}a_{\mathbf{k}}^{(r)}\right\} - B'\sum_{r,\mathbf{k}}S_r\cos(\theta_r)a_{\mathbf{k}}^{(r)\dagger}a_{\mathbf{k}}^{(r)}, \quad (4)$$

where $\mathbf{k}$ is the momentum vector. Here, $z_{rs}^{(u)}$ is the number of SL s sites coupled by the interaction $J_{rs}^{(u)}$ to a site on SL r, and u denotes the multiple possible interactions from SL r to SL s. For example, a FM with a single SL can have both nearest-neighbor and next-nearest-neighbor interactions with $u = 1$ and 2. We have also defined $\Gamma_{\mathbf{k}}^{rs(u)} = 1/z_{rs}^{(u)}\sum_{\mathbf{d}}\mathrm{e}^{-\mathrm{i}\mathbf{k}\cdot\mathbf{d}^{(u)}}$ with $\mathbf{d}^{(u)} = \mathbf{R}_j - \mathbf{R}_i$ where $\mathbf{R}_i$ on SL r and $\mathbf{R}_j$ on SL s are coupled by the exchange $J_{rs}^{(u)}$. Note that $\Gamma_{\mathbf{k}=0}^{rs(u)} = 1$ and $\Gamma_{\mathbf{k}}^{rs(u)} = \Gamma_{-\mathbf{k}}^{rs(u)*} = \Gamma_{\mathbf{k}}^{sr(u)*}$. Finally, G_1^{rs} and G_2^{rs} are rotation coefficients that depend only on the moment angles for the specific SL (described in appendix A).

To determine the SW frequencies $\omega_{\mathbf{k}}$, we solve the equation-of-motion for the vectors $\mathbf{v}_{\mathbf{k}} = [a_{\mathbf{k}}^{(1)}, a_{\mathbf{k}}^{(1)\dagger}, a_{\mathbf{k}}^{(2)}, a_{\mathbf{k}}^{(2)\dagger}, \ldots, a_{\mathbf{k}}^{(s_t)}, a_{\mathbf{k}}^{(s_t)\dagger}]$, which may be written in terms of the $2s_t \times 2s_t$ matrix $\underline{M}(\mathbf{k})$ as

$$\mathrm{i}\mathrm{d}\mathbf{v}_{\mathbf{k}}/\mathrm{d}t = -\left[\underline{H}_2, \mathbf{v}_{\mathbf{k}}\right] = \underline{M}(\mathbf{k})\mathbf{v}_{\mathbf{k}}, \quad (5)$$

where s_t is the number of spin SLs. The SW frequencies are then determined from the condition $\mathrm{Det}[\underline{M}(\mathbf{k}) - \omega_{\mathbf{k}}\underline{I}] = 0$, where only positive frequencies are retained.

The structure factor in a magnetic system describes the intensity expected from experiment for SW modes with resolution-limited width [27]. In the case of a standard FM with identical nearest-neighbor interactions, the structure factor is constant throughout k-space. However, as the spins cant, the wavevector dependence becomes important.

Local stability in a magnetic system requires two conditions: (1) all SW frequencies must be real for every $\mathbf{k}$ and (2) the SW weights $W_{\mathbf{k}}^{(t)}$ must be positive. The weights are given by the coefficients of the delta functions in the spin–spin correlation function

$$S(\mathbf{k},\omega) = \tfrac{1}{2}\left[S^{+,-}(\mathbf{k},\omega) + S^{-,+}(\mathbf{k},\omega)\right] + S^{z,z}(\mathbf{k},\omega) = \sum_t W_{\mathbf{k}}^{(t)}\delta(\omega - \omega_{\mathbf{k}}^{(t)}), \quad (6)$$

where ω is the eigenfrequency for the spin-wave [27, 28] and the sum over t means a sum over all SW modes. The total number of transverse or longitudinal SW modes in the first Brillouin zone equals the number of magnetic SLs s_t.

Generally, the spin–spin correlation function is

$$S^{\alpha,\beta}(\mathbf{k},\omega) = \frac{1}{N}\int\mathrm{d}t\mathrm{e}^{-\mathrm{i}\omega t}\sum_{i,j}\mathrm{e}^{\mathrm{i}\mathbf{k}\cdot(\mathbf{R}_j-\mathbf{R}_i)}\left\langle\mathbf{S}_i^\alpha(0)\mathbf{S}_j^\beta(t)\right\rangle, \quad (7)$$

where $\alpha, \beta = +, -$, and z [27, 28]. The transverse terms ($\alpha, \beta = +, -$) correspond to $S^{+,-}(\mathbf{k},\omega)$ and $S^{-,+}(\mathbf{k},\omega)$ in $S(\mathbf{k},\omega)$, while the longitudinal term $S^{z,z}(\mathbf{k},\omega)$ with $\alpha = \beta = z$ is only nonzero when the system is canted. Here, $\langle\mathbf{S}_i^\alpha(0)\mathbf{S}_j^\beta(t)\rangle = \langle(\underline{U}_i^{-1}\tilde{\mathbf{S}}_i(0))^\alpha(\underline{U}_j^{-1}\tilde{\mathbf{S}}_j(t))^\beta\rangle$ is rotated from the local-moment frame to the global frame. It should be noted that a SW mode may be purely longitudinal or transverse, with weight in the $\langle zz\rangle$ or $\langle\pm\mp\rangle$ channel exclusively. Alternatively, a SW mode may contain weight in both channels. We provide examples of both possibilities in our discussion of the generalized Villain model in section 3.

By expanding and solving for the spin Green's functions, we can write $S^{\alpha,\beta}(\mathbf{k},\omega)$ as

$$S^{\alpha,\beta}(\mathbf{k},\omega) = -\frac{4}{\pi}\lim_{\delta\to0}\mathrm{Im}\left(\mathrm{Tr}\left(\underline{G}(\mathbf{k},\omega+\mathrm{i}\delta)\underline{C}_{\alpha\beta}\right)\right), \quad (8)$$

where

$$\underline{G}(\mathbf{k},\omega+\mathrm{i}\delta) = \int_0^{1/T}\mathrm{d}\tau\ \mathrm{e}^{\mathrm{i}\omega_l\tau}\underline{g}^{\mathbf{k}}(\tau)\Big|_{\mathrm{i}\omega_l\to\omega+\mathrm{i}\delta}, \quad (9)$$

$\omega_l = 2l\pi T$, and $C^{nm}_{\alpha\beta}$ are the rotational coefficients for the canted moments, which depend only on the angles θ and ψ (described in appendix A). Here $n = 2r - 1, 2r$ for SL r and

$$g^{\mathbf{k}}_{nm}(\tau) = -\langle T_\tau \mathbf{v}_{n\mathbf{k}}(\tau)\mathbf{v}_{m\mathbf{k}}\rangle, \tag{10}$$

where $v_{n\mathbf{k}}(\tau) = e^{H_2\tau} v_{n\mathbf{k}} e^{-H_2\tau}$. Using the equations-of-motion of $\mathbf{v}_{n\mathbf{k}}(\tau)$, the Green's function matrix can be solved as

$$G_{nm}(\mathbf{k}, \omega + i\delta) = \left[\frac{-1}{(\omega + i\delta)\underline{I} - \underline{M}(\mathbf{k})}\underline{N}\right]_{nm}, \tag{11}$$

where $\underline{I}$ is an $2s_t \times 2s_t$ identity matrix and $\underline{N}$ is an $2s_t \times 2s_t$ matrix defining the commutation relations such that $[\mathbf{v}_{n,\mathbf{k}}, \mathbf{v}_{m,\mathbf{k}}] = N_{nm}$.

From the commutation relation, $[S^+_i, S^-_j] = 2S_z\delta_{ij}$, one can determine the net magnetic moment from the sum rule

$$\langle S_z\rangle = \int_{-\infty}^{\infty} d\omega S_z(\mathbf{k}, \omega), \tag{12}$$

where $S_z(\mathbf{k}, \omega) = \frac{1}{2}(S^{+-}(\mathbf{k}, \omega) - S^{-+}(\mathbf{k}, \omega))$. Note that $S_z(\mathbf{k}, \omega)$ is not the same as the longitudinal spin–spin correlation function, $S^{z,z}(\mathbf{k}, \omega)$. Since $\langle S_z\rangle$ does not depend on $\mathbf{k}$, neither does the right-hand side of equation (12).

3. The generalized Villain model: classical energy and phase boundaries

To demonstrate the rotational technique described above, we examine the GVM′ described in figure 1. This model neglects anisotropy, but includes an applied magnetic field. The introduction of γ into the GVM′ expands the overall interaction phase space, which can illuminate some of the interesting phenomena seen within the cuprate and manganite systems. An overall analysis of the numerical and analytical results will provide detailed information about the GVM′, as well as a unique look at the nature of the spin phases as one moves through the interaction phase space.

While the general rotational Hamiltonian describes interactions between spin sites with moment rotations in both the xz (θ) and xy (ψ) planes, the GVM′ constrains the moment angles to rotations in the xz-plane, which greatly simplifies the technique. Therefore, spin–spin interactions can be denoted as angle pairs (θ_a, θ_b). This constraint also allows the SW frequencies for the GVM′ to be determined analytically.

Through an examination of the classical energy, we determine the energy boundaries for each spin configuration. From equation (2), the classical energy of SC1 is

$$E_0^{(SC1)} = \frac{JS^2}{2}\big(\eta\cos(2\theta_b) - \cos(2\theta_a) - 2\gamma\cos(\theta_a - \theta_b) - B'(\cos(\theta_a) + \cos(\theta_b))\big). \tag{13}$$

Minimizing $E_0^{(SC1)}$ with respect to θ_a and θ_b yields the relations

$$\begin{aligned} \sin(2\theta_a) + \gamma\sin(\theta_a - \theta_b) + \tfrac{1}{2}B'\sin(\theta_a) = 0, \\ \eta\sin(2\theta_b) + \gamma\sin(\theta_a - \theta_b) - \tfrac{1}{2}B'\sin(\theta_b) = 0. \end{aligned} \tag{14}$$

Assuming that (θ_a, θ_b) satisfy these criteria, the first order terms from the Hamiltonian $H_1^{(SC1)}$ will vanish. At zero field

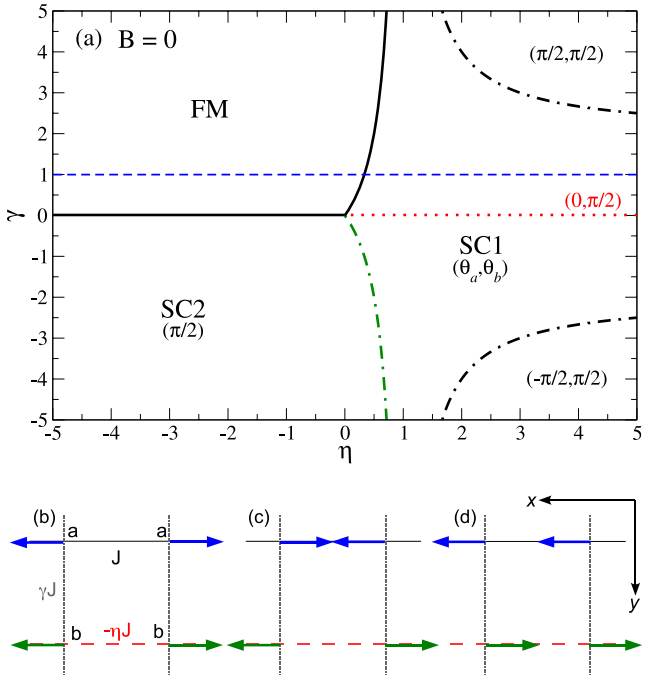

Figure 2. (a) The phase diagram for the GVM′ at $B = 0$ in the interaction space of γ and η. The green dash-dotted line indicates the phase boundary between SC1 and SC2 and the blue dashed line shows the sub-space of the GVM′ ($\gamma = 1$). (b)–(d) Pictorial representations of the (b) $(\pi/2, \pi/2)$ and (c) $(-\pi/2, \pi/2)$ limit regions (black dash-dotted line in (a)) of the SC1 phase, and (d) the SC2 phase at zero field.

and in the limit of large η, the local moments cant toward the angles $(\tan^{-1}(\gamma/\sqrt{4-\gamma^2}), \pi/2)$. In the limit $\gamma \to 1$, equations (13) and (14) agree with the results of [24], where θ_a and θ_b approach angles smaller than $\pi/6$ and $\pi/2$, respectively. With increasing η and $|\gamma|$, the zero-field SC1 phase approaches one of the planar phases shown in figures 2(b) and (c).

By linearizing equation (14), we obtain the phase boundary between the SC1 and FM phases:

$$B' = 2\Big(\eta - \gamma - 1 \pm \sqrt{\gamma^2 + (\eta + 1)^2}\Big). \tag{15}$$

In the limit $\gamma \to 1$, this gives the relation obtained by Gabay *et al* [29]. Solving equation (15) for γ, we find the phase boundaries

$$\gamma = \pm\frac{(4 + B')(4\eta - B')}{4(2 - 2\eta + B')}. \tag{16}$$

Figure 2(a) shows the phase diagram for the zero-field GVM′. Here, the blue dotted line goes along $\gamma = 1$, where the critical value, $\eta_c = 1/3$, is consistent with previous work [3].

In zero field, SC1 with angles $(0, \pi)$ is equivalent to SC2 with $\alpha = \pi/2$. However, due to the absences of anisotropy in the GVM′, a magnetic field in the z direction immediately produces a spin flop into the xy plane with the spins canted towards the z-axis. This configuration corresponds to SC2 with $\alpha < \pi/2$. Figure 2(d) shows the SC2 phase at zero field, where $\alpha = \pi/2$ throughout the region. Equation (16) gives the field dependence of the SC1/FM boundary.

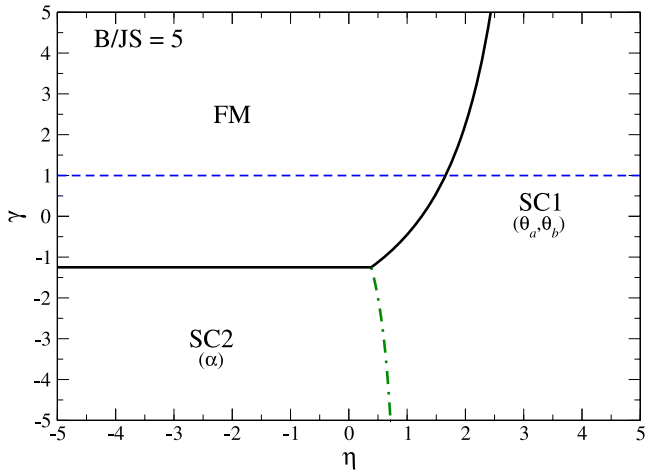

Figure 3. Phase diagram for the GVM′ at $B' = B/JS = 5$ in the interaction space of γ and η. The green dash-dotted line indicates the phase boundary between SC1 and SC2. The blue dashed line shows the sub-space of the GVM′ where $\gamma = 1$.

To find the field-dependent boundaries for the SC2 phase, we examine the classical energy

$$E_0^{(SC2)} = \frac{JS^2}{2}\big(\eta - 1 - 2\gamma\cos(2\alpha) - 2B'\cos(\alpha)\big). \quad (17)$$

At zero field, SC2 has the same energy as SC1. However, SC2 has the lower energy when a magnetic field is applied, so it does not follow the same field dependence as SC1. By minimizing the energy, we obtain the SC2 angle

$$\cos(\alpha) = -\frac{B'}{4\gamma}, \quad (18)$$

which depends only on B' and γ. Consequently, the SC2/FM phase boundary is given by $B' = -4\gamma$ and the SC1/SC2 phase boundary is given by

$$\gamma = -\frac{2\eta}{(\eta - 1)}, \quad (19)$$

which is shown by the green dash-dotted line in figures 2(a) and 3. This reveals that the SC1/SC2 boundary does not depend on field. As the magnetic field increases, the FM phase expands along this boundary, creating a triple point at $\eta = B'/(B' + 8)$ and $\gamma = -B'/4$. The expansion of the FM phase space with field is clearly illustrated in figure 3, where $B' = 5$.

4. Generalized Villain model: spin-waves and structure factors

Using the methods described in section 2, we apply this new technique to the spin dynamics of the GVM′ in the three regions of the phase diagram (FM, SC1, and SC2). Since the environments surrounding the moments at sites a_1 and a_2 are equivalent, they can be considered part of the same sub-lattice. Similarly, for sites b_1 and b_2. The SW frequencies can be determined analytically for all phases. The SF intensities will be obtained for a more complete picture of the system. In the FM and zero-field SC2 phases, we solve the SF intensities analytically. However, due to the added complexity of the nonzero-field SC2 and SC1 phases, those intensities must be determined numerically.

The second order GVM′ Hamiltonian can be written as

$$H_2 = JS\sum_{\mathbf{k},r,s}\Big(a_{\mathbf{k}}^{(r)\dagger}a_{\mathbf{k}}^{(s)}A_{\mathbf{k}}^{(r,s)} + (a_{-\mathbf{k}}^{(r)}a_{\mathbf{k}}^{(s)} + a_{-\mathbf{k}}^{(r)\dagger}a_{\mathbf{k}}^{(s)\dagger})B_{\mathbf{k}}^{(r,s)}\Big), \quad (20)$$

where $A_{\mathbf{k}}^{(r,s)}$ and $B_{\mathbf{k}}^{(r,s)}$ are coefficients that describe the interactions while $r, s = a$ or b represent the two SLs [24]. The resulting SW frequencies can be expressed analytically using the modified coefficients for the different spin configurations, with expressions given in appendix B.

4.1. The FM phase

Both the SW frequencies and SF intensities of the FM phase can be obtained analytically. The SW frequencies are described by

$$\omega_{\mathbf{k}}^{\pm} = B + JS\big(2\gamma + (\eta - 1)(\cos(k_x) - 1) \pm R_{1\mathbf{k}}\big), \quad (21)$$

where

$$R_{1\mathbf{k}} = \sqrt{(\eta + 1)^2(1 - \cos(k_x))^2 + 4\gamma^2\cos(k_y)^2} \quad (22)$$

and the lattice constant a has been set to 1. In the limit $k_x = 0$, $\omega_{\mathbf{k}} = B + 2\gamma JS(1 \pm \cos(k_y))$ only depends on γJ, which is consistent with previous results [18, 23–25]. As a function of γ, η, and $\mathbf{k}$, the SF intensities are given by

$$W_{\mathbf{k}}^{\pm} = \frac{R_{1\mathbf{k}} \mp 2\gamma\cos(k_y)}{R_{1\mathbf{k}}}. \quad (23)$$

This describes the SF intensities for both the high (+) and low (−) frequency SW.

Figure 4 shows $W^{\pm}(k_x, \eta)$ with $\gamma = 3$ and $k_y = 0$ for the high (a) and low (b) SW modes of the FM phase. If γ is held constant, the plot forms a saddle, where the intensity at $\eta = -1$ is the maximum throughout k_x/π. If $\gamma \geqslant 1$, then this maximum is constant over k_x, which is consistent with the standard two-dimensional FM. When $\gamma > 1$, the maximum displays non-linear behavior as k_x goes to π. The sharpness of the saddle depends on γ. As γ approaches 0, the saddle sharpens to a delta function at $\eta = -1$, while increasing γ flattens the saddle. The mode with the maximum intensity is also determined by γ. If $\gamma > 0$, then the low-frequency mode dominates the intensity. The opposite is true for negative γ. As η departs from -1 the SF intensity becomes more dependent on k_x/π and the intensity decreases. Therefore, even though the system is a two-dimensional FM, the non-equivalent interactions create a unique intensity pattern. When the intensities are summed over the high and low frequencies, the total intensity is constant throughout $\mathbf{k}$. This demonstrates that the complex interactions distribute the intensity between the two SW branches, but the total intensity still remains constant as in the standard ferromagnet.

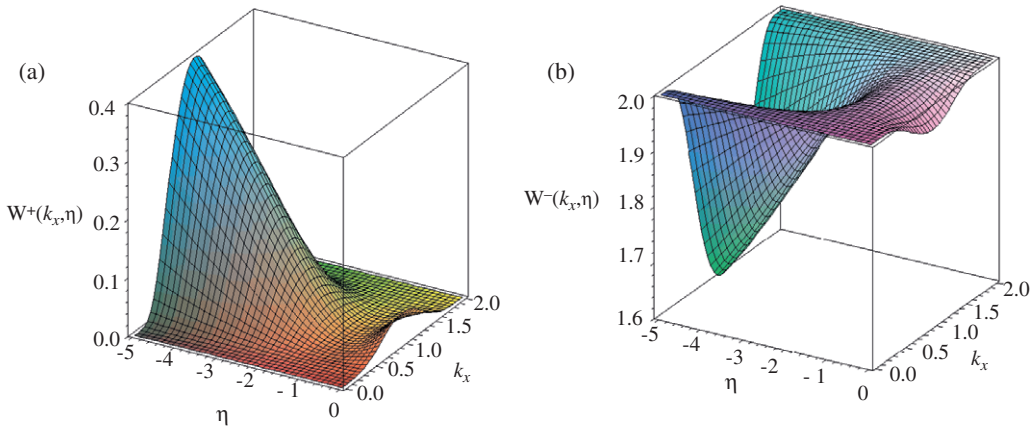

Figure 4. $W(k_x, \eta)$ for the (a) high- and (b) low-frequency modes of the FM state with $\gamma = 3$ and $k_y = 0$. This shows the full spectrum from $\eta = -5, \ldots, 0$.

4.2. The SC1 phase

The SC1 region is described by angles (θ_a, θ_b) that are given by equation (14). The SW frequency coefficients for the GVM are given by equation (B.1) in appendix B. In this section, we present the SW frequencies and SF intensities for varying γ, η, and B' to give a representative cross-section of the CAF region. Due to the complexity of the SF intensities, they have been determined numerically.

The region $\gamma = 1$ has been examined in great detail in [18] and [24], where the SW intensities increase dramatically as $(k_x/\pi, k_y/\pi)$ approaches (1, 0). A more moderate shift in the intensity is seen along $(0, k_y/\pi)$. As shown below, similar features are observed as γ is increased.

Figure 5 shows the longitudinal and transverse components for the high and low SW frequencies and SF intensities at zero field with $\eta = 4$ and $\gamma = 1, \ldots, 4$. The higher-frequency modes have a lower intensity at (1, 0) and higher intensity at (0, 1) with exception for transverse component of $\gamma = 1$ at (0, 1). The lower SW frequencies tend to decrease in the $(k_x/\pi, 0)$ direction and increase in the $(0, k_y/\pi)$ direction. This difference arise because the exchange γJ is along the y direction. As γ increases, the shift in the intensities along the $(0, k_y/\pi)$ direction become more pronounced. As γ decreases, the SW intensity along the $(0, k_y/\pi)$ direction disappears as the FM and AF chains become decoupled.

As shown in figure 2(a), the corners of the zero-field phase diagram consist of two planar regions sketched in figures 2(b) and (c). A magnetic field causes the spins in both regions to cant. In figure 5, we investigate the transition from the SC1 phase into this planar regime. While the SW frequencies do not show much overall difference, the SF intensities do show a

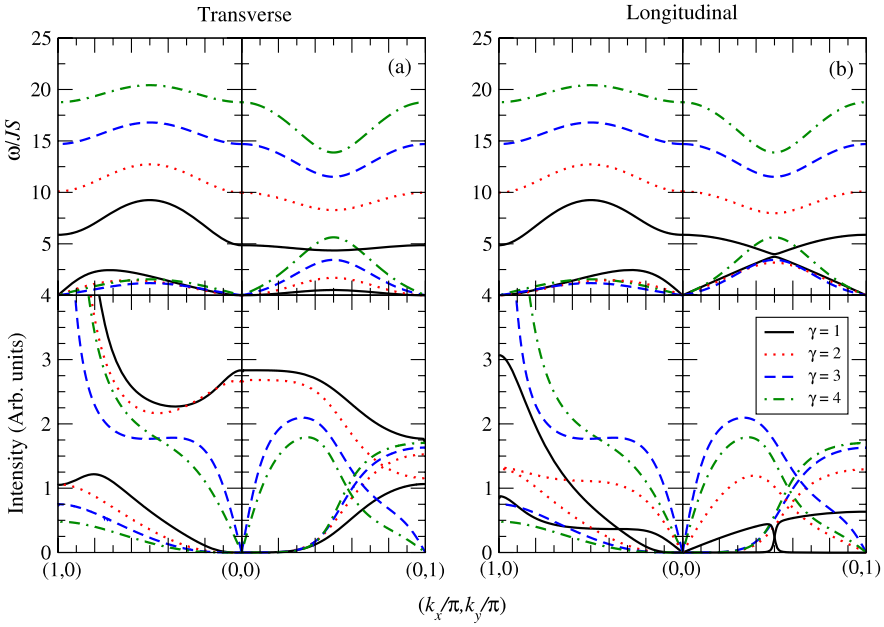

Figure 5. (a) The transverse component high- and low-frequency SW modes at $B' = 0$ and $\eta = 4$ for $\gamma = 1, \ldots, 4$ as function of $(k_x/\pi, k_y/\pi)$. Their corresponding SF intensities over the same values are shown below. (b) The longitudinal component high- and low-frequency SW modes and intensities that are activated by the canting of the local moment. The higher-frequency modes have a lower intensity at (1, 0) and higher intensity at (0, 1) with the exception for the transverse component of $\gamma = 1$ at (0, 1).

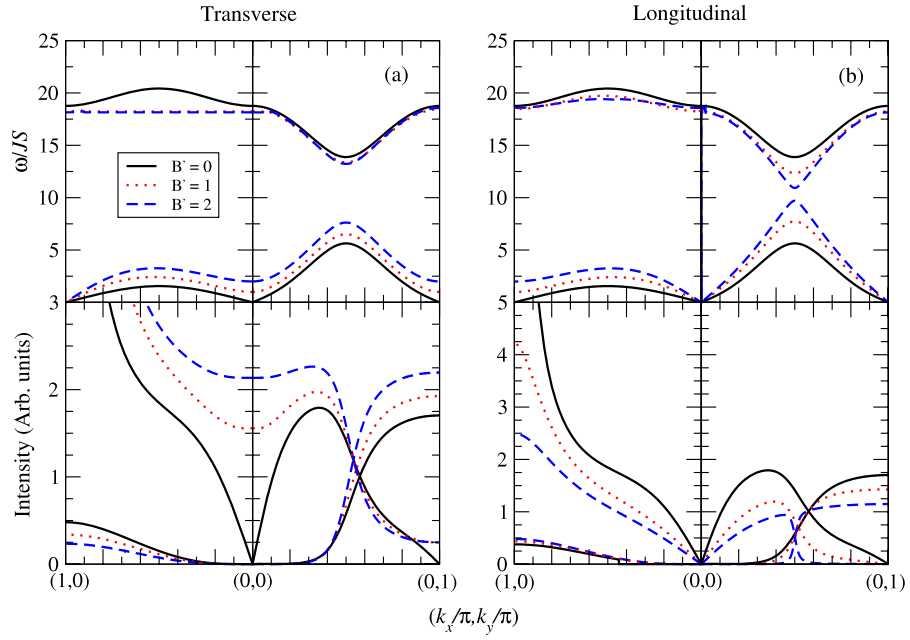

Figure 6. (a) The transverse component to the high- and low-frequency SW modes for $B' = 0, \ldots, 2$ with $\eta = \gamma = 4$ as function of $(k_x/\pi, k_y/\pi)$. The corresponding SF intensities over the same values are shown below. (b) Longitudinal component to the high- and low-frequency SW modes that are activated by the canting of the local moments. The higher-frequency modes have a lower intensity at (1, 0) and higher intensity at (0, 1).

distinct change that would help distinguish between the canted SC1 phase and its planar limit. The change seen in figure 5 clearly shows the loss of intensity for the SW modes at (0, 0) after entering the planar region with $\gamma > 8/3$. Note that the transverse and longitudinal components become identical in the planar phase having equal weight, but for $\gamma > 8/3$ in the canted phase the SW modes are either purely transverse or longitudinal. An overall frequency spectra is a superposition of both modes, where the intensities for the transverse terms correspond to $S^{+,-}(\mathbf{k}, \omega)$ and $S^{-,+}(\mathbf{k}, \omega)$ and the longitudinal term is $S^{z,z}(\mathbf{k}, \omega)$. They are displayed separately to illustrate the individual components.

Once a magnetic field is applied, the SW frequencies increase due to the enhanced stiffness of the local moment. Figure 6 shows the progression of the high and low SW frequencies and their corresponding SF intensities as the applied magnetic field increases from $B' = 0, \ldots, 2$ with $\eta = \gamma = 4$. This transition is clearly evident in the low-frequency intensity at (0, 0), which becomes nonzero as the field increases and the spins cant towards the z-axis.

4.3. The SC2 phase

The angle α was given in terms of the field and γ by equation (18). Although α does not depend on η, changing η does modify the SW frequencies and SF intensities. The SW frequencies for this phase can be determined analytically by the equation given by Fishman [24] assuming different coefficients (equations (B.2) and (B.3) in appendix B). As with the SC1, the SF intensities must be determined numerically. However, as for the FM phase, the zero-field intensities of the SC2 phase with $\alpha = \pi/2$ can be solved analytically.

In zero field, the SW frequencies are

$$\omega_{\mathbf{k}}^{\pm} = \sqrt{R_{2\mathbf{k}}^{+} R_{2\mathbf{k}}^{-}} \pm (\eta + 1)(1 - \cos(k_x)), \tag{24}$$

where

$$R_{2\mathbf{k}}^{\pm} = (\eta - 1)(\cos(k_x) - 1) + 2\gamma(-1 \pm \cos(k_y)). \tag{25}$$

The SF intensities are given analytically by

$$W_{\mathbf{k}} = \sqrt{\frac{R_{2\mathbf{k}}^{+}}{R_{2\mathbf{k}}^{-}}}. \tag{26}$$

Even though the angles of the local moments do not change throughout the zero-field phase, the SW frequencies and SF intensities depend on the interaction parameters, γ and η, where the zero-field intensity for each branch in equation (24) is the same.

Figure 7 shows the SW frequencies and SF intensities for the SC2 phase with $\gamma = \eta = -2$ as the applied field increases from $0, \ldots, 10$ in steps of 4. This figure helps further investigate the field-induced canting in this phase, where it is demonstrated that the transition from the planar SC2 phase into a field-induced canted phase and then finally into the FM phase as α goes from $\pi/2$ to 0. Once in the FM phase, the SW modes increase linearly with field while the SF intensity remains the same. Each mode of the SC2 phase has both longitudinal and transverse components. This is different from the SC1 phase, where the longitudinal modes are separate from the transverse.

5. Conclusion

In an attempt to understand the nature of competing FM and AF interactions and canted spin moments, we presented a

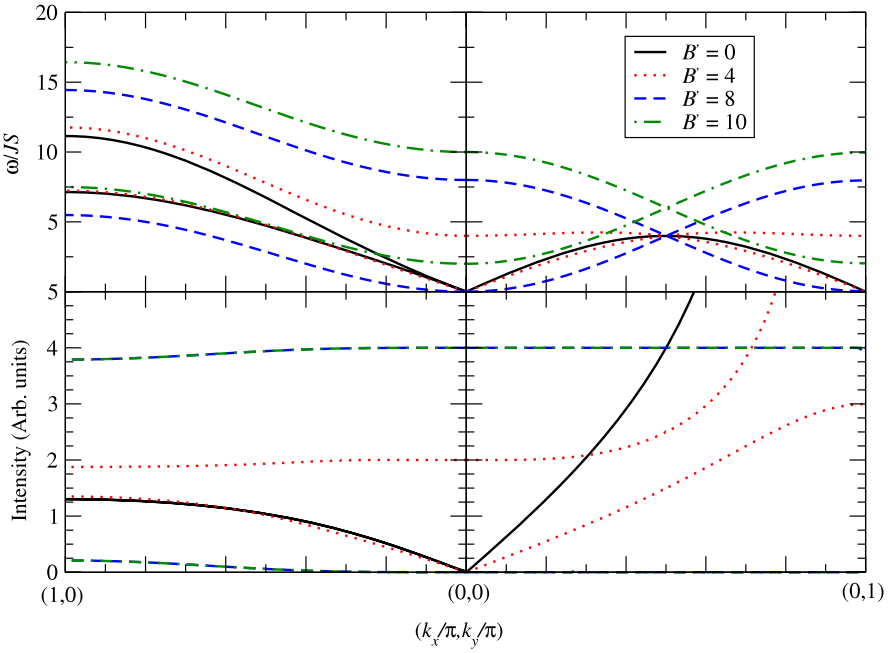

Figure 7. High- and low-frequency SW modes for $B' = 0, \ldots, 10$ with $\eta = \gamma = -2$ as function of $(k_x/\pi, k_y/\pi)$. Corresponding SF intensities over the same values. The higher-frequency modes have a lower intensity at (1, 0) and (0, 1).

spin rotation technique for the determination of the static and dynamic properties for any periodic magnetic spin system. Using Euler angles, we determined the interactions within the local frame of reference for each spin, and applied these rotations to a Holstein–Primakoff expansion to determine the classical energy and SW frequencies. A Green's function technique was used to determine the SF intensities for any eigenfrequency of the system.

This technique was then applied to the generalized Villain model (GVM), which has been further generalized by introducing a varying interchain coupling. By studying the affects of this new interaction, we hope to gain a deeper understanding of frustrated magnetic systems. To obtain the phase boundaries and dynamics throughout the GVM′, we introduced two spin configurations: SC1 and SC2.

With the phase space established, the SW frequencies and SF intensities for the different phases were determined. The SW frequencies were determined analytically through the whole phase space. In most cases, the SF intensities were determined numerically. However, we were able to provide an analytical equation for the FM and zero-field SC2 phase that showed how the SF intensity depends on the interactions. Using these quantities, we presented a cross-section of the phase space to give an overall picture of the GVM′.

We hope that this technique will prove useful in the understanding of many different non-collinear magnetic systems. Magnetic heterostructures as well as frustrated AFs such as $CuFeO_2$ are some of the systems that may be studied with this technique.

Acknowledgments

We would like to acknowledge helpful conversations with Satoshi Okamoto and Wayne Saslow. This research was sponsored by the Laboratory Directed Research and Development Program of Oak Ridge National Laboratory, managed by UT-Battelle, LLC for the US Department of Energy under Contract No. DEAC05-00OR22725, and by the Division of Materials Science.

Appendix A. Rotation coefficients

Using Euler rotations with angles (θ and ψ) [26], each spin $\mathbf{S}_i$ is rotated into its local frame of reference using $\tilde{\mathbf{S}}_i = \underline{U}_i \mathbf{S}_i$, where the rotation matrix, $\underline{U}_i$, is given by

$$\underline{U}_i = \begin{vmatrix} \cos(\theta_i)\cos(\psi_i) & \cos(\theta_i)\sin(\psi_i) & -\sin(\theta_i) \\ -\sin(\psi_i) & \cos(\psi_i) & 0 \\ \sin(\theta_i)\cos(\psi_i) & \sin(\theta_i)\sin(\psi_i) & \cos(\theta_i) \end{vmatrix}. \quad \text{(A.1)}$$

When examining the interaction between two spin operators, the overall rotation from one reference frame to another is

$$\underline{U}_i \underline{U}_j^{-1} = \begin{vmatrix} F_{xx}^{ij} & F_{xy}^{ij} & F_{xz}^{ij} \\ F_{yx}^{ij} & F_{yy}^{ij} & F_{yz}^{ij} \\ F_{zx}^{ij} & F_{zy}^{ij} & F_{zz}^{ij} \end{vmatrix}, \quad \text{(A.2)}$$

where $F_{\alpha\beta}^{ij}$ can be obtained from equation (A.1). It should be noted that there are s_t different unitary matrices, one for each magnetic SL r. The rotation coefficients for the generalized second order Hamiltonian (equation (4)) are

$$\begin{aligned} G_1^{rs} &= -\tfrac{1}{2}(F_{xx}^{rs} + F_{yy}^{rs} - \mathrm{i}(F_{xy}^{rs} - F_{yx}^{rs})) \\ G_2^{rs} &= -\tfrac{1}{2}(F_{xx}^{rs} - F_{yy}^{rs} - \mathrm{i}(F_{xy}^{rs} + F_{yx}^{rs})). \end{aligned} \quad \text{(A.3)}$$

When calculating the SW intensities, one needs to multiply each element in the spin Green's function matrix by a rotation coefficient that describes the transverse and

longitudinal contributions to the SF. The rotational coefficients of the transverse components $\langle \mathbf{S}_r^{\pm}(0)\mathbf{S}_s^{\mp}(t)\rangle$ are given by

$$\begin{aligned}
2C_{\pm,\mp}^{2s-1,2r-1} &= C_{xx,xx}^{rs} + C_{yx,yx}^{rs} - (C_{xy,xy}^{rs} + C_{yy,yy}^{rs}) \\
&\mp (C_{xx,yy}^{rs} - C_{yx,xy}^{rs}) \mp (C_{xy,xy}^{rs} - C_{yy,xx}^{rs}) \\
&+ \mathrm{i}\big(\mp (C_{xx,yx}^{rs} - C_{yx,xx}^{rs}) \pm (C_{xy,yy}^{rs} - C_{yy,xy}^{rs}) \\
&- (C_{xx,xy}^{rs} + C_{yx,yy}^{rs}) - (C_{xy,xx}^{rs} + C_{yy,yx}^{rs})\big) \\
2C_{\pm,\mp}^{2s,2r-1} &= C_{xx,xx}^{rs} + C_{yx,yx}^{rs} - (C_{xy,xy}^{rs} + C_{yy,yy}^{rs}) \\
&\pm (C_{xx,yy}^{rs} - C_{yx,xy}^{rs}) \pm (C_{xy,xy}^{rs} - C_{yy,xx}^{rs}) \\
&+ \mathrm{i}\big(\mp (C_{xx,yx}^{rs} - C_{yx,xx}^{rs}) \pm (C_{xy,yy}^{rs} - C_{yy,xy}^{rs}) \\
&+ (C_{xx,xy}^{rs} + C_{yx,yy}^{rs}) + (C_{xy,xx}^{rs} + C_{yy,yx}^{rs})\big) \\
2C_{\pm,\mp}^{2s-1,2r} &= C_{xx,xx}^{rs} + C_{yx,yx}^{rs} + (C_{xy,xy}^{rs} + C_{yy,yy}^{rs}) \\
&\mp (C_{xx,yy}^{rs} - C_{yx,xy}^{rs}) \pm (C_{xy,xy}^{rs} - C_{yy,xx}^{rs}) \\
&+ \mathrm{i}\big(\mp (C_{xx,yx}^{rs} - C_{yx,xx}^{rs}) \mp (C_{xy,yy}^{rs} - C_{yy,xy}^{rs}) \\
&- (C_{xx,xy}^{rs} + C_{yx,yy}^{rs}) + (C_{xy,xx}^{rs} + C_{yy,yx}^{rs})\big) \\
2C_{\pm,\mp}^{2s,2r} &= C_{xx,xx}^{rs} + C_{yx,yx}^{rs} + (C_{xy,xy}^{rs} + C_{yy,yy}^{rs}) \\
&\pm (C_{xx,yy}^{rs} - C_{yx,xy}^{rs}) \mp (C_{xy,xy}^{rs} - C_{yy,xx}^{rs}) \\
&+ \mathrm{i}\big(\mp (C_{xx,yx}^{rs} - C_{yx,xx}^{rs}) \mp (C_{xy,yy}^{rs} - C_{yy,xy}^{rs}) \\
&+ (C_{xx,xy}^{rs} + C_{yx,yy}^{rs}) - (C_{xy,xx}^{rs} + C_{yy,yx}^{rs})\big),
\end{aligned} \tag{A.4}$$

where $C_{ab,cd}^{rs} \equiv U_{ab}^{-1r} U_{cd}^{-1s}$ is defined in terms of the inverse of the rotation matrix elements. Note that r and s denote a specific SL dependent on angles θ and ψ. The rotational coefficients for the longitudinal component $\langle \mathbf{S}_r^{z}(0)\mathbf{S}_s^{z}(t)\rangle$ are given by

$$\begin{aligned}
2C_{z,z}^{2s-1,2r-1} &= C_{zx,zx}^{rs} - C_{zy,zy}^{rs} - \mathrm{i}(C_{zx,zy}^{rs} + C_{zy,zx}^{rs}) \\
2C_{z,z}^{2s,2r-1} &= C_{zx,zx}^{rs} + C_{zy,zy}^{rs} + \mathrm{i}(C_{zx,zy}^{rs} + C_{zy,zx}^{rs}) \\
2C_{z,z}^{2s-1,2r} &= C_{zx,zx}^{rs} + C_{zy,zy}^{rs} - \mathrm{i}(C_{zx,zy}^{rs} + C_{zy,zx}^{rs}) \\
2C_{z,z}^{2s,2r} &= C_{zx,zx}^{rs} - C_{zy,zy}^{rs} + \mathrm{i}(C_{zx,zy}^{rs} + C_{zy,zx}^{rs}).
\end{aligned} \tag{A.5}$$

Appendix B. Spin-wave frequency coefficients

When $\gamma = 1$, the second order Hamiltonian (equation (20)) and SW frequencies were determined analytically by Fishman in [24]. For the GVM′ Hamiltonian with general γ, the coefficients for SC1 are

$$\begin{aligned}
A_{\mathbf{k}}^{(a,a)} &= 2\cos(2\theta_a) + 2\gamma\cos(\theta_a - \theta_b) - 2\cos^2(\theta_a)\cos(k_x) \\
&\quad + B'\cos(\theta_a) \\
A_{\mathbf{k}}^{(a,b)} &= A_{\mathbf{k}}^{(b,a)} = -2\gamma\cos^2((\theta_a - \theta_b)/2)\cos(k_y) \\
A_{\mathbf{k}}^{(b,b)} &= 2\gamma\cos(\theta_a - \theta_b) - 2\eta\cos(2\theta_b) \\
&\quad + 2\eta\cos^2(\theta_b)\cos(k_x) + B'\cos(\theta_b) \\
B_{\mathbf{k}}^{(a,a)} &= \sin^2(\theta_a)\cos(k_x) \\
B_{\mathbf{k}}^{(a,b)} &= B_{\mathbf{k}}^{(b,a)} = -2\gamma\sin^2((\theta_a - \theta_b)/2)\cos(k_y) \\
B_{\mathbf{k}}^{(b,b)} &= -\eta\cos^2(\theta_b)\cos(k_x),
\end{aligned} \tag{B.1}$$

while the coefficients for SC2 are given by

$$\begin{aligned}
A_{\mathbf{k}}^{(a,a)} &= 2(1 + \gamma\cos(\theta_a - \theta_b) - \cos(k_x)) + B'\cos(\theta_a) \\
A_{\mathbf{k}}^{(a,b)} &= A_{\mathbf{k}}^{(b,a)} = -2\gamma\cos^2((\theta_a - \theta_b)/2)\cos(k_y) \\
A_{\mathbf{k}}^{(b,b)} &= 2(\gamma\cos(\theta_a - \theta_b) - \eta + \eta\cos(k_x)) + B'\cos(\theta_b) \\
B_{\mathbf{k}}^{(a,a)} &= 0 \\
B_{\mathbf{k}}^{(a,b)} &= B_{\mathbf{k}}^{(b,a)} = -2\gamma\sin^2((\theta_a - \theta_b)/2)\cos(k_y) \\
B_{\mathbf{k}}^{(b,b)} &= 0.
\end{aligned} \tag{B.2}$$

The SW frequencies are given in terms of $A_{\mathbf{k}}^{(r,s)}$ and $B_{\mathbf{k}}^{(r,s)}$, where $r, s = a$ or b. The frequencies for the transverse modes are given as

$$\begin{aligned}
\omega_{\mathbf{k}} = \frac{JS}{\sqrt{2}}\Big\{ & A_{\mathbf{k}}^{(a,a)2} + A_{\mathbf{k}}^{(b,b)2} + 2\left(A_{\mathbf{k}}^{(a,b)2} - B_{\mathbf{k}}^{(a,b)2}\right) \\
& - 4\left(B_{\mathbf{k}}^{(a,a)2} + B_{\mathbf{k}}^{(b,b)2}\right) \pm R_{3\mathbf{k}}\Big\}^{-1/2},
\end{aligned} \tag{B.3}$$

where

$$\begin{aligned}
R_{3\mathbf{k}}^2 = {} & 4\big(A_{\mathbf{k}}^{(a,a)2} + A_{\mathbf{k}}^{(b,b)2} - 4\big(B_{\mathbf{k}}^{(a,a)2} + B_{\mathbf{k}}^{(b,b)2}\big)\big) \\
& \times \big(A_{\mathbf{k}}^{(a,b)2} - B_{\mathbf{k}}^{(a,b)2}\big) + \big(A_{\mathbf{k}}^{(a,a)2} - A_{\mathbf{k}}^{(b,b)2} \\
& - 4\big(B_{\mathbf{k}}^{(a,a)2} - B_{\mathbf{k}}^{(b,b)2}\big)\big)^2 + 8\big(A_{\mathbf{k}}^{(a,a)} A_{\mathbf{k}}^{(b,b)} + 4B_{\mathbf{k}}^{(a,a)} B_{\mathbf{k}}^{(b,b)}\big) \\
& \times \big(A_{\mathbf{k}}^{(a,b)2} + B_{\mathbf{k}}^{(a,b)2}\big) - 32A_{\mathbf{k}}^{(a,b)} B_{\mathbf{k}}^{(a,b)} \\
& \times \big(A_{\mathbf{k}}^{(a,a)} B_{\mathbf{k}}^{(b,b)} + A_{\mathbf{k}}^{(b,b)} B_{\mathbf{k}}^{(a,a)}\big),
\end{aligned} \tag{B.4}$$

and $\pm$ denote the higher-and lower-frequency modes. The longitudinal mode frequencies for SC1 are obtained from these expressions by $k_x \to k_x + \pi$.

References

[1] Kittel C 1987 *Quantum Theory of Solids* (New York: Wiley)
[2] Villain J 1977 *J. Phys. C: Solid State Phys.* **10** 1717
[3] Berge B, Diep H T, Ghazali A and Lallemand P 1986 *Phys. Rev.* B **34** 3177
[4] Khrapai V S, Deviatov E V, Shashkin A A, Dolgopolov V T, Hastreiter F, Wixforth A, Campman K L and Gossard A C 2000 *Phys. Rev. Lett.* **84** 725
[5] Sánchez D, Brey L and Platero G 2001 *Phys. Rev.* B **64** 235304
[6] Lazarovits B, Ujfalussy B, Szunyogh L, Stocks G M and Weinberger P 2004 *J. Phys.: Condens. Matter* **16** S5833
[7] van Duijn J, Attfield J P, Watanuki R, Suzuki K and Heenan R K 2003 *Phys. Rev. Lett.* **90** 087201
[8] Coffey D, Rice T M and Zhang F C 1991 *Phys. Rev.* B **44** 10112
[9] Shekhtman L, Aharony A and Entin-Wohlman O 1993 *Phys. Rev.* B **47** 174
[10] Jorgensen J D, Chmaissem O, Shaked H, Short S, Klamut P W, Dabrowski B and Tallon J L 2001 *Phys. Rev.* B **63** 054440
[11] Cao G, McCall S, Zhou Z X, Alexander C S, Crow J E, Guertin R P and Mielke C H 2001 *Phys. Rev.* B **63** 144427
[12] Nakamura K and Freeman A J 2002 *Phys. Rev.* B **66** 140405(R)
[13] For an overview of phase separation in the manganites see Moreo A, Yunoki S and Dagotto E 1999 *Science* **283** 2034 Dagotto E, Hotta T and Moreo A 2001 *Phys. Rep.* **233** 1
[14] Adams C P, Lynn J W, Mukovskii Y M, Arsenov A A and Shulyatev D 2000 *Phys. Rev. Lett.* **85** 3954

[15] Koo T Y, Kiryukhin B, Sharma P A, Hill J P and Cheong S-W 2001 *Phys. Rev.* B **64** 220405
[16] Waldman O 2007 *Phys. Rev.* B **75** 012415
[17] Saslow W M 1983 *Phys. Rev.* B **27** 6873
[18] Saslow W M and Erwin R 1992 *Phys. Rev.* B **45** 4759
[19] Carlson E W, Yao D X and Campbell D K 2004 *Phys. Rev.* B **70** 064505
[20] Walker L R and Walstedt R E 1980 *Phys. Rev.* B **22** 3816
[21] Walker L R and Walstedt R E 1977 *Phys. Rev. Lett.* **38** 514
[22] Rastelli E, Tassi A and Reatto L 1979 *Physica* B **97** 1
[23] Fishman R S 2004 *Phys. Rev.* B **70** 012403
[24] Fishman R S 2004 *J. Phys.: Condens. Matter* **16** 5483
[25] Fishman R S 2004 *Phys. Rev.* B **70** 140402(R)
[26] Arfken G B and Weber H J 2001 *Mathematical Methods for Physicists* (New York: Academic)
[27] Squires G L 1996 *Introduction to the Theory of Thermal Neutron Scattering* (New York: Dover)
[28] Balcar E and Lovesey S W 1989 *Theory of Magnetic Neutron and Photon Scattering* (New York: Oxford University Press)
[29] Gabay M, Garel T, Parker G N and Saslow W M 1989 *Phys. Rev.* B **40** 264